Optics Communications 588 (2025) 131944

Contents lists available at ScienceDirect

Optics Communications

journal homepage: www.elsevier.com/locate/optcom

Self and joint intensity statistics of Laguerre–Gaussian modes propagating in air turbulence

K.O. Bastian [a], S. Pokharel [a], M. Mahdavifar [a,b], O. Korotkova [a,*]

[a] Department of Physics, University of Miami, 1320 Campo Sano Ave, Coral Gables, FL, 33146, United States
[b] School of Physics, University of the Witwatersrand, Private Bag 3, Johannesburg, 2050, South Africa

ARTICLE INFO

Keywords:
Orbital Angular Momentum correlation
Cross-spectral density
Intensity–intensity correlation
Scintillation index
Two-point correlation

ABSTRACT

The results of an experimental campaign on propagating several Laguerre–Gaussian (LG) beams with trivial radial order and their random sequences through the controlled-air turbulence are presented. Various statistical moments of the fluctuating intensity of a single LG mode and the mode-to-mode correlations and their derivatives are found. The mode-to-mode intensity correlations revealed the appearance of robust ring-like structures depending in size on the mode index difference. The experimental results were verified with the help of numerical simulations.

1. Introduction

The interest in the Orbital Angular Momentum (OAM) in modern optics was largely generated by seminal work [1] showing that the Laguerre–Gaussian (LG) laser modes are its intrinsic carriers. It was soon suggested that the LG modes can be employed in optical communications due to their ability to securely transmit large amounts of information by means of OAM mode multiplexing [2]. Such systems were later experimentally realized over practical near-ground free-space links [3] and underwater [4].

The effects of atmospheric turbulence on power coupling among the LG modes, and hence, on communication channel capacity, was well understood from early theoretical studies [5]. This analysis was recently extended from weak to strong turbulence regime in [6,7] by means of split-step computer simulations.

A number of individual statistics of LG beams also received considerable attention. The robustness of topological charges associated with the LG modes in various regimes of atmospheric turbulence was revealed by means of phase-optics simulations with multiple phase screens [8]. The spatial spreading of the LG modes due to atmospheric turbulence was numerically analyzed in [9,10] by a similar simulation scheme with a single and multiple phase screens.

The laboratory simulations of LG mode based communication links were developed with the help of the spatial light modulators (SLM) for weak turbulence with a single phase screen [11] and for strong turbulence with a calibrated pair of screens [12]. Other statistics of LG modes were also reported [13]. Some simulation studies concerned the LG modes interaction with anisotropic turbulence which is commonly present in the boundary layer within several meters above the ground. For example, in [14] the spiral spectrum and mode coupling of the LG modes in such turbulence was discussed. Very few experimental campaigns were reported so far in air-generated turbulence that specifically target intensity statistics of the LG modes. In [15] the beam quality and stability of several LG modes were investigated at distances up to 600 m outdoors. It was also shown in [16] that in controlled air turbulence the scintillation index of the LG beams can be suppressed with fast (several kHz) modulation of the radial mode.

This paper offers comprehensive analysis of experimental data obtained from the passage of several static LG beams and their fast-modulated random sequences, after interaction with the controlled air turbulence. We aim to scrutinize various statistics relating to fluctuating intensity of these beams, in particular, average value, normalized variance, beam wander radius, and self- and cross-mode intensity correlations.

2. Experiment

An experiment generating the LG modes and their randomized sequences, passing them through the hot-air turbulence, and recording their fluctuating intensities was conducted at the University of Miami campus, in the optics lab and the hallway of the Department of Physics. Fig. 1 shows the schematic diagram of the optical setup. A collimated laser beam of wavelength 405 nm, 40 mW of exit power and radius 1 mm was passed through the variable-strength ND filter F, expanded by a telescope T, and sent onto the Digital Mirror Device (DMD, Texas

* Corresponding author.
E-mail address: o.korotkova@miami.edu (O. Korotkova).

https://doi.org/10.1016/j.optcom.2025.131944
Received 8 August 2024; Received in revised form 28 April 2025; Accepted 29 April 2025
Available online 14 May 2025

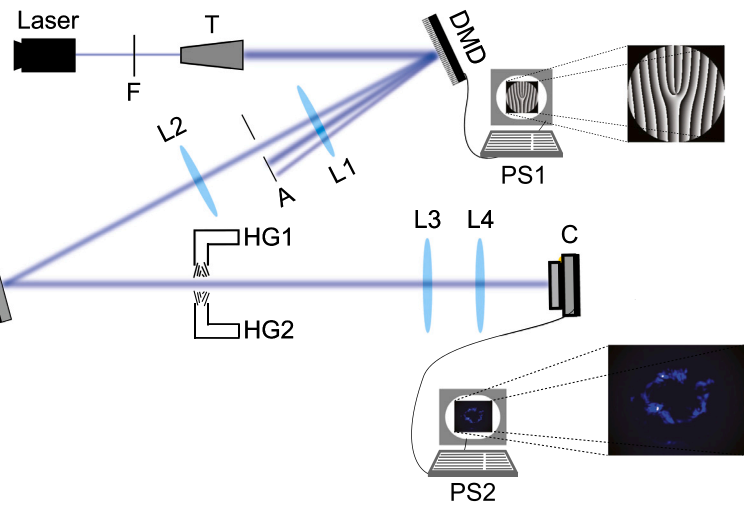

Fig. 1. Experimental setup for the LG mode generation, passage in hot-air simulated atmospheric turbulence and recording.

Instruments) at angle 12° loaded with either a constant LG mode with zero radial order with or their random sequences. The DMD patterns were controlled from computer PS1. The LG modes

$$LG_0^l(\rho,\phi) = \frac{1}{\omega}\sqrt{\frac{2}{\pi|l|!}}\left(\frac{\rho\sqrt{2}}{\omega}\right)^{|l|} \exp\left[-\frac{\rho^2}{\omega^2}\right] \exp\left[il\phi\right], \tag{1}$$

were assigned to the DMD screen via the fork phase-only distributions. Here l is the OAM index, ω is the beam size at the waist, ρ and ϕ are the radial and angular coordinates in the polar system.

The first-order diffraction mode was then filtered out with the help of the 4-f system consisting of lenses L1 ($f = 10$ cm) and L2 ($f = 25$ cm), and diaphragm A. The diffractive modes from the DMD grating were first focused by lens L1, then the first mode (carrying the LG modes) was selected by diaphragm A and collimated by lens L2.

Right after reflection from mirror M at the exit of the optics lab, the beams were passed through a small air volume between a pair of heat guns (Porter Cable, PC1500HG) precisely facing each other. After interacting with the heat guns generated air turbulence the beam was sent to a 20-meter channel in the presence of negligible air turbulence that was due to the hall air-conditioning system. Such air-gun induced turbulent volume was previously characterized with the thermocouple array for mean temperature and spatial covariance function [17].

The beam then was collimated into the CMOS camera C (Thorlabs, DCC3240C, 1280 × 1024 pixels, pixel size 5.3 μm × 5.3 μm) after passing through the system of lenses L3 ($f = 25$ cm) and L4 ($f = 2.5$ cm). The recorded sequences of images were stored on computer PS2 in the multi-page .jpg format. For recording of each data point three independent measurements separated in time were obtained and then combined for averaging. For each data point, a folder of $N = 1000$ images was generated. Both stationary LG_0^l modes ($l = 0, \dots, 5$) and the random sequences of modes $l = 1$ and $l = 2$ were used with different speeds of the DMD, in the range from 100 Hz to 4 kHz.

The stability of the experimental setup was sufficient for the purpose of beam generation, its interaction with turbulence and its recording by camera. The generation of the LG modes with the help of the DMD was performed on a vibration-free optical table. The only highly vibrating unit, the heat gun stage, was located sufficiently far from both the beam source and the camera. We note that in this work we have not used any experimental interferometric procedures that would indeed require enhanced stability measures. The measurements relating to each LG mode were repeated three times on the same setup. They returned excellent correlation. The repeatability of the results was also checked with another dataset recorded with different ranges and heat-gun strength to return the same trends in data but slightly different numerical values (not included in reported results).

3. Data processing

Before processing all the images were cut to the lowest pixel dimension, i.e., 1024 pixels, by removing 118 pixels on the left side and 138 pixels on the right side (for better centering). Hence, Figs. 2, 3 and 5–7 shown below have size 1024 × 1024 pixels. Let the pixel (x, y) intensity of image i in an image sequence be $I(x, y, i)$. Then this pixels' intensity averaged over the total number N of realizations in the image folder can be calculated as

$$\langle I(x,y)\rangle = \frac{1}{N}\sum_{i=1}^{N} I(x,y,i). \tag{2}$$

Unless normalized, the intensity is presented in the figures in pixel level units (0–255) as measured by the CMOS camera.

The pixel-resolved variance of fluctuating intensity is given by expression

$$\mathrm{Var}[I(x,y)] = \frac{1}{N}\sum_{i=1}^{N}\left[I(x,y,i) - \langle I(x,y)\rangle\right]^2. \tag{3}$$

The normalized version of the variance, i.e.,

$$\sigma_I^2(x,y) = \frac{\mathrm{Var}[I(x,y)]}{\langle I(x,y)\rangle^2}. \tag{4}$$

can be used to characterize the single-pixel intensity fluctuations.

Next, we calculate the beam wander for the individual modes, $l = 0, \dots, 5$. To locate the center of the beam we first apply the cutoff of the normalized variance, at value 10% from the maximum intensity level. The variance (and not the average intensity) is used because of its more pronounced boundaries. For all the intensity values greater than the cutoff, the pixel's x and y coordinates are recorded and the maximum and minimum values of the intensity are obtained from this set. Using these values, we then find the pixel coordinates of the center of the beam denoted by x_0 and y_0:

$$x_0 = \frac{x_{max} + x_{min}}{2}, \quad y_0 = \frac{y_{max} + y_{min}}{2}. \tag{5}$$

Further, for each frame $i = 1, \dots, N$ the x and y coordinates of the beam intensity centroid are calculated from formulas

$$I_c(x,i) = \frac{\sum_{x=1}^{x_{max}} x \cdot I(x,y,i)}{I_{tot}(i)}, \quad I_c(y,i) = \frac{\sum_{y=1}^{y_{max}} y \cdot I(x,y,i)}{I_{tot}(i)}, \tag{6}$$

where the total intensity for each frame is

$$I_{tot}(i) = \sum_{x=1}^{x_{max}}\sum_{y=1}^{y_{max}} I(x,y,i) \tag{7}$$

with $x_{max} = y_{max} = 1024$.

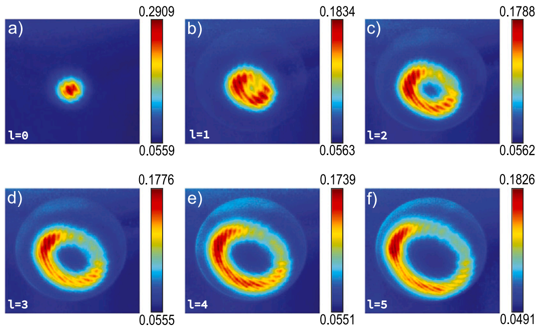

Fig. 2. Density plots of average intensity for individual LG modes, $l = 0, \dots, 5$.

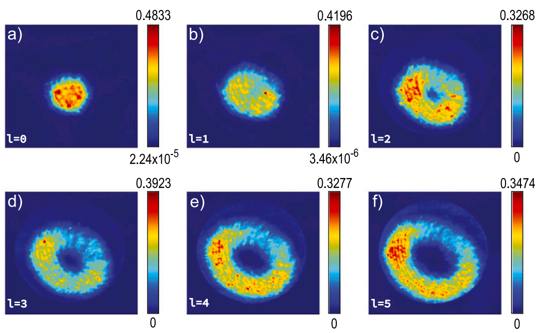

Fig. 3. Density plots of normalized variance for individual LG modes, $l = 0, \dots, 5$.

The beam wander radius of each frame is then calculated from distance expression

$$r(i) = \sqrt{[I_c(x,i) - x_0]^2 + [I_c(y,i) - y_0]^2}, \tag{8}$$

and, finally, the beam wander of the whole sequence becomes

$$\sigma_r = \sqrt{\frac{\sum_{i=1}^{N}[r(i) - \bar{r}_i]^2}{N}}, \tag{9}$$

where, $\bar{r}_i$ is an average beam wander radius

$$\bar{r}_i = \frac{1}{N}\sum_{i=1}^{N} r(i). \tag{10}$$

In order to evaluate the correlation of each pixel's intensity in a frame i with that of the central pixel $I(x_0, y_0, i)$ (in the same frame) we first calculate its average $\langle I(x_0, y_0)\rangle$ from Eq. (2). Then the covariance of the intensity with respect to the central pixel takes form

$$\begin{aligned}&\mathrm{Cov}[I(x,y)I(x_0,y_0)]\\&\quad = \frac{1}{N}\sum_{i=1}^{N}[I(x,y,i) - \langle I(x,y)\rangle]\\&\quad \times [I(x_0,y_0,i) - \langle I(x_0,y_0)\rangle].\end{aligned} \tag{11}$$

The two-point intensity correlation is then calculated with normalization

$$\beta(x,y,x_0,y_0) = \frac{\mathrm{Cov}[I(x,y), I(x_0,y_0)]}{\langle I(x,y)\rangle \cdot \langle I(x_0,y_0)\rangle}. \tag{12}$$

The all-pixel correlation analysis of the pair of image sequences can be carried out via the discrete version of the 2D convolution operation. It is computationally more efficient to employ the convolution theorem of Fourier transforms and evaluate this quantity with the help of the 2D FFT operator via expression

$$\gamma_{1,2}(x,y) = \sum_{i=1}^{N} \mathcal{F}^{-1}[\mathcal{F}^*[I_1(x,y)] \cdot \mathcal{F}[I_2(x,y)]], \tag{13}$$

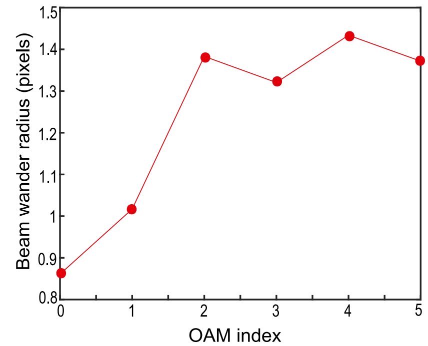

Fig. 4. Beam wander radius σ_r in units being pixels of the LG modes ($l = 0, \dots, 5$).

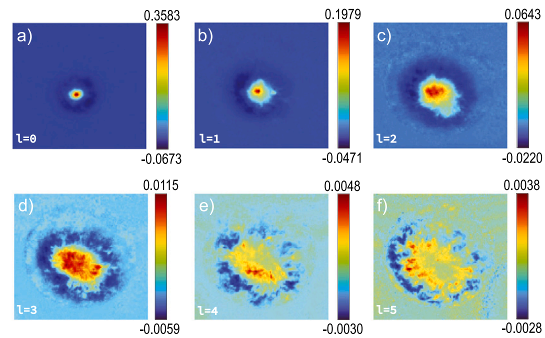

Fig. 5. Density plots of $\beta(x, y, x_0, y_0)$ for the structured beams with different OAM indices, $l = 0, \dots, 5$.

where $\mathcal{F}$ and $\mathcal{F}^{-1}$ are the direct and inverse 2D Fourier transforms and star denotes complex conjugation.

4. Numerical results and discussion

We will first present the numerical results relating to the single LG mode statistics. Fig. 2 shows the average intensity distributions of LG modes $l = 0, \dots, 5$ calculated from Eq. (2), normalized to the maximum level. The ring-like shapes appear starting from mode $l = 1$, then become larger and thinner but level off with size as l grows to 5. At the same time, the maximum intensity values gradually decrease.

Fig. 3 shows the normalized intensity variance distributions calculated from Eq. (4) for the same modes as Fig. 2. Although structurally the variance resembles the average intensity, it occupies somewhat larger regions while its small-scale patterns appear to be much noisier. The summary of beam wander analysis of modes $l = 0, \dots, 5$ based on Eqs. (5)–(9), is presented in Fig. 4. Beam wander, calculated in coordinates with units being pixels, from the centroid deviations across several frames, is the lowest for $l = 0$ and increases with the OAM index, until leveling off for modes $l \geq 2$.

Fig. 5 presents the two-point correlation $\beta(x, y, x_0, y_0)$ (each pixel with the central pixel) of beams with $l = 0, \dots, 5$, calculated from Eqs. (10)–(11). All six distributions involve both positive and negative correlations. As l increases both maximum (positive) and minimum (negative) correlations gradually tend to zero. For the lower modes, $l \leq 3$, the maximum value of β occurs in the beam center. For higher modes, $l \geq 4$ a correlation ring is formed and the maximum value of β belongs to a point on the ring. With the growing l the radii of the ring-like correlations monotonically increase. Also, with the increasing mode, the averaging quality decreases resulting in more pronounced noise patterns.

Fig. 6 summarizes the all-pixel correlations γ_{l_1,l_2} of pairs of OAM modes ($l_1, l_2 = 0, \dots, 5$), calculated from Eq. (11). The self and joint correlations occupy the diagonal and off-diagonal positions of the table,

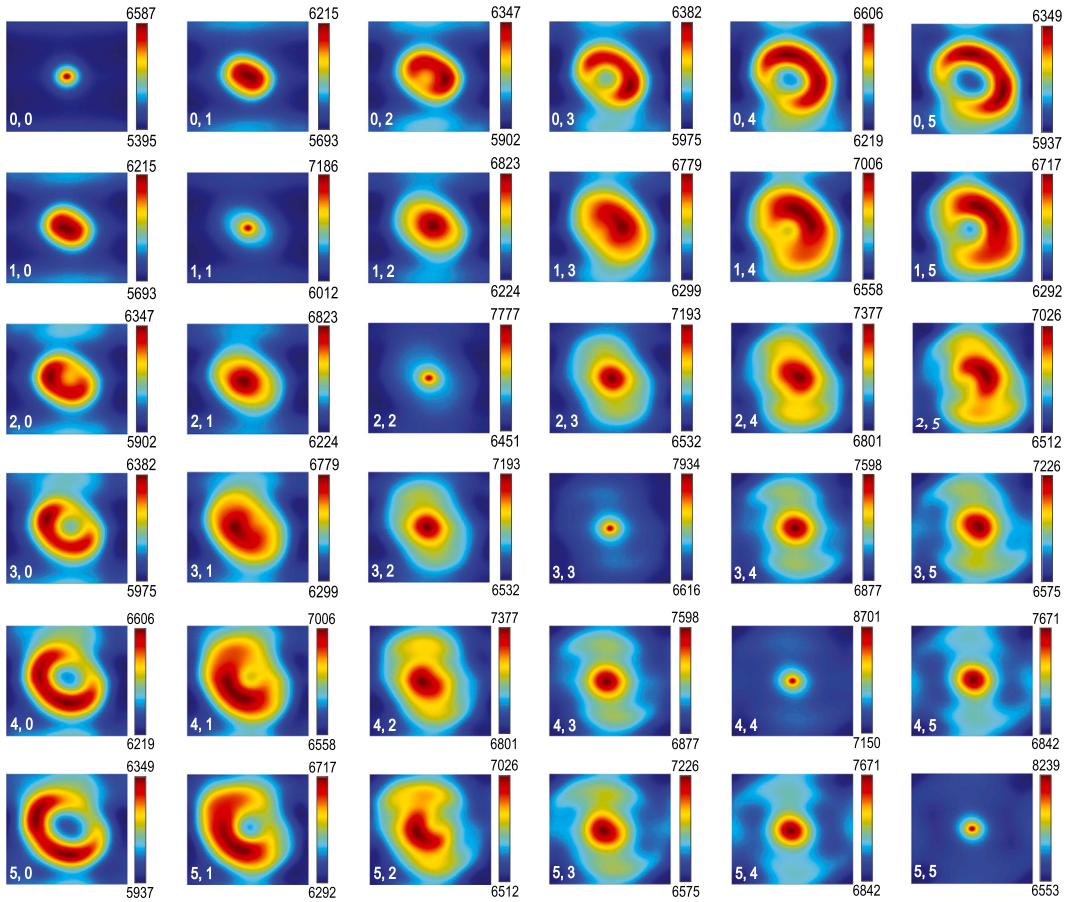

Fig. 6. Density plots of intensity–intensity correlations of LG modes with various OAM indices ($l_1, l_2 = 0, \dots, 5$).

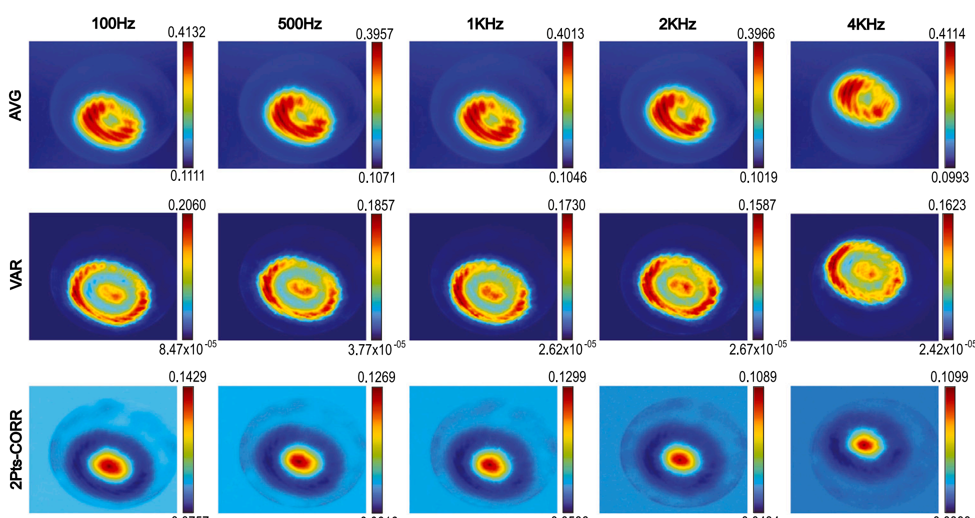

Fig. 7. Density plots of average intensity, normalized variance, and two-point correlations of a random sequence of LG modes $l_1 = 1$ and $l_2 = 2$.

respectively. The off-diagonal elements (l_1, l_2) and (l_2, l_1) are precise reflections of each other about the optical axis, making the whole table symmetric. The self-correlations of all modes have maxima in the center of the patterns. They all show precisely symmetric distributions and are very narrow. As for the joint correlations, the structure depends on the individual indices and their differences. For example, correlations (l_1, l_2) form very pronounced rings for $|l_1 - l_2| > 2$ expanding with the increase of mode index difference. On the other hand, correlations with small index difference $|l_1 - l_2| \leq 2$ show no ring structure still having maximum in the center but relatively wide distributions. The off-diagonal elements are generally not having self-symmetric patterns.

The emergence of ring-like shaped intensity–intensity correlations in different LG laser modes after their interaction with atmospheric turbulence resembles a recent experimental result [18] pertaining to the same statistics of LG modes measured after scattering through a diffuser. The rings of [18] were very narrow and their radii were precisely related to difference $|l_1 - l_2|$. This was due to a number of reasons, for example, a Gaussian random process governing scattering

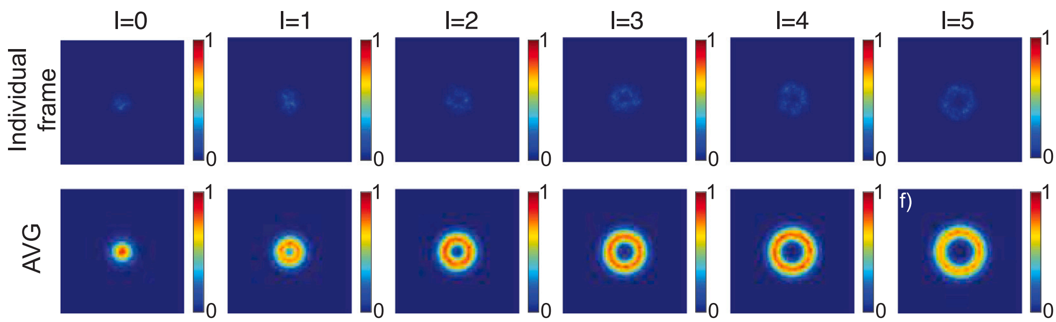

Fig. 8. Wave-optics simulations of LG modes, $l = 0, 1, \dots, 5$. Density plots of: individual realizations of intensity (top row); averaged intensity distributions (bottom row).

and far field (well developed) scattering. The rings reported here cannot be observed for all mode pairs, and they have larger widths. This could be due to the fact that turbulent random process is not Gaussian and that the beams are not measured in the far field. We also notice that unlike the rings in [18] obtained for the LG modes passage through a single and exactly the same diffuser screen, the rings in Fig. 6 are the results of mode interacting with two different sequences of turbulence screens. Namely, the individual realizations of the turbulent screens are different, while, of course, the statistics are the same. Thus, this ring structure appearing in the joint intensity correlations of the LG modes remains very robust in the turbulent air.

Fig. 7 shows the average intensity, the variance, and the two-point correlation of a beam formed with two random sequences of OAM modes $l_1 = 1$ and $l_2 = 2$, for several values of DMD cycling rate. The probability of the two modes was set to be equal. As is evident from the figure, the average intensity of a beam (first row) is doughnut-like in shape with the partially filled center. This is the direct consequence of addition of the two average intensities shown in Figs. 2(B) and (C). The normalized variance of a two LG mode random sequence (second row) is shaped as a combination of narrow central maximum and a larger ring. The highest values of the scintillation index are consistent with the edges of the corresponding average intensity distributions. Note that the two-mode variance is not directly relating to those of the individual modes in Figs. 3(B) and (C). Further, the two-point correlation $\beta(x, y, m, n)$ (each pixel with the central pixel) of the two LG-mode random sequence shown in the bottom row does structurally represent the averaged correlations for modes $l_1 = 1$ and $l_2 = 2$ in Fig. 5(B) and (C). The range of the correlation is increased and the distributions become considerably smoother. Different columns in the figure represent the DMD speeds which do not substantially affect the results of the average intensity and the variance. However, with the increasing DMD rate, the two-point correlation is seen to reduce in range.

5. Wave-optics simulations

We will now compare the experimental data analyzed in the previous section with the results of numerical computation obtained with the help of the wave-optics simulation and the Kolmogorov model of atmospheric turbulence [19]. Since the turbulence of the experiment was in its weak regime, it was sufficient to apply a single phase screen at the mid-path of the heatgun-camera link, for obtaining each beam's realization [20]. First, the sequences of 200 realizations were recorded for each of the six LG modes ($l = 0, 1, \dots, 5$) using different turbulence screen sequences. In other words, neither each LG mode realization nor different LG mode realizations have interacted with the same turbulence realization. Then the intensity averages and correlations were calculated in MATLAB, all normalized to their maximum values.

The simulation results are displayed in Figs. 8 and 9, using the following beam and turbulence parameters: a propagation distance of $z = 20$ m, a wavelength of $\lambda = 0.450 \times 10^{-6}$ m, an initial beam width of $w_0 = 3$ cm, while the refractive index structure parameter was set as $C_n^2 = 5\times 10^{-16}$ m$^{-2/3}$. We note that the used C_n^2 numerical value mimics the path-averaged turbulence strength along the path (not that within the heatgun airflow, being several orders of magnitude higher).

Fig. 8 presents both individual realizations (top row) and the averaged intensity distributions after beam's interaction with turbulence (bottom row), for various LG modes, $l = 0, 1, \dots, 5$. All the sub-figures were normalized by the maximum intensity level. The reason behind the fact that the individual realizations (top row) appear much weaker as a whole is that only at one or a very few pixels the maximum average is reached and these pixels are not visible. The turbulence screen generator had the tip-tilt procedure enabled, hence the rings seen in the top row (short-exposure frames) are typically smaller than those in the bottom row (long-exposure frames). The results of Fig. 8 are similar to those shown in Fig. 2. Fig. 9 illustrates the cross-correlation between different OAM modes, performed in MATLAB with the help of the same 2D FFT correlator as used in data processing section.

The whole table in Fig. 9 is in excellent agreement with that in Fig. 6. Indeed, while the self-correlations (diagonal elements) have narrow Gaussian-like distributions, the joint correlations become larger at a small separation of OAM indices ($|l - m|$ is small) but then gradually transform to rings as this separation grows ($|l - m|$ is larger). The diagonal elements do not show substantial dependence of l, just like in Fig. 6. Further, the correlation of modes $l = 0$ and $l = 5$ delivers the most pronounced ring, again confirming the corresponding result of Fig. 6. We note that self-correlations appear having much lower maximum intensities. This is due to the fact that the maximum as reached at a few pixels that are not visible. To highlight it we also provided the insert for the (0,0) correlation. Thus, the results of the experiment and of the numerical simulation are in excellent agreement.

6. Summary

An experimental campaign was carried out on recording the fluctuating intensity of several zero-radial-order LG modes and their random sequences, after their interaction with controlled hot-air turbulence. The analysis of various intensity statistics was performed. One of the major outcomes of our study is the non-trivial behavior of the single-point, two-point and all-point intensity correlations, both for a single LG mode and a pair of modes. In particular, the all-point intensity correlations calculated with the help of the 2D FFT-based procedure for modes $l_1, l_2 = 0, \dots, 5$ and summarized in Fig. 6, has revealed that while for $l_1 = l_2$ the intensity–intensity correlations have ordinary structure (Gaussian-like distributions), those for $l_1 \neq l_2$ form rings. The size of the rings increases with the increase in the value of $|l_1 - l_2|$ and becomes very pronounced for $|l_1 - l_2| > 2$. This phenomenon is similar to that produced on the LG modes scattering in [18]. Another interesting observation was made on comparison of the intensity statistics calculated for static modes and for their random sequences. We found very little dependence of the size, the structure and the dynamic range of all the processed statistics on the cycling rate of the DMD, although it was changed in the large range between 100 Hz and 4 kHz, i.e., covering

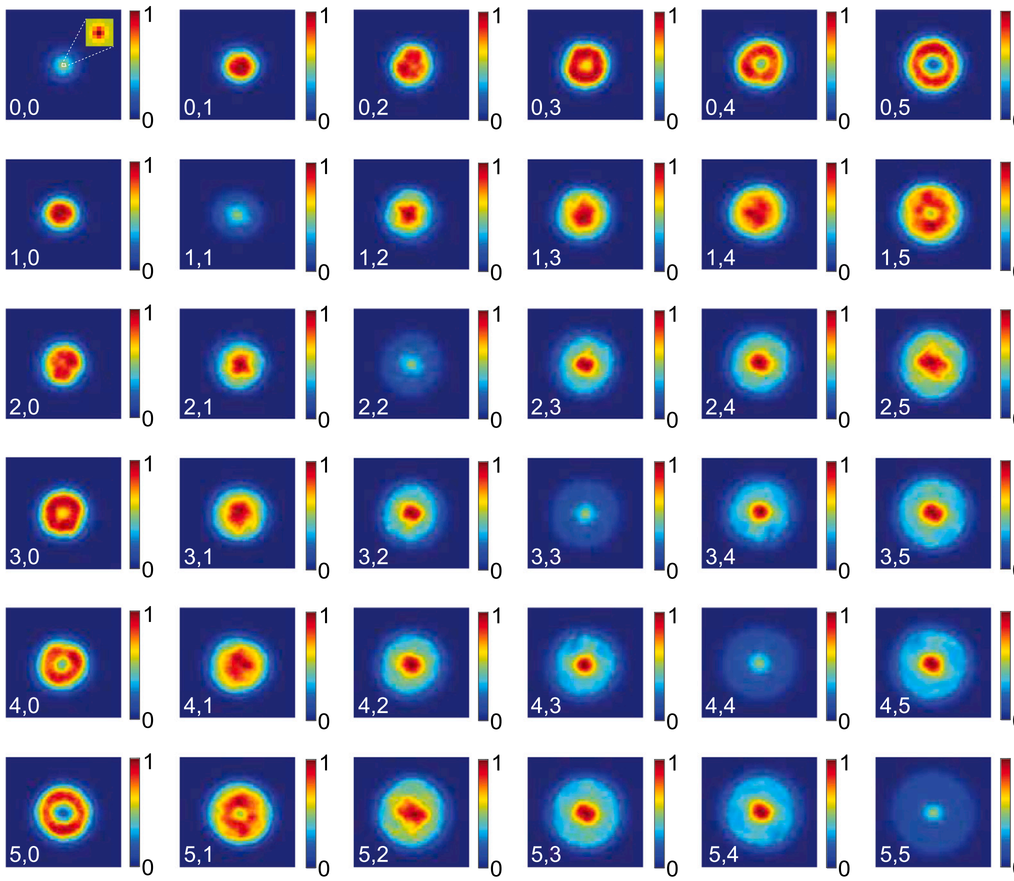

Fig. 9. Wave-optics simulations: density plots of intensity–intensity correlations of the LG modes with various OAM indices, $l = 0, 1, \ldots, 5$.

various regimes of temporal averaging. Our current result is different from that in [16] where radial mode modulation of the LG modes was performed and was shown to substantially affect the intensity statistics.

The results of the experimental campaign were verified with the help of wave-optics based simulation and showed very close agreement. In particular, the most important observation of this work, the ring-like structured intensity–intensity correlation of different OAM modes, has shown the identical trend in simulation.

The appearance of the rings in the joint intensity–intensity correlations of pairs of the LG modes, with the size depending on the OAM index difference, may be leveraged in a new type of a free-space laser communication protocol requiring mitigation of turbulence. At present a typical OAM-based communication system is based on encoding of information into the individual LG modes. Since the structure of the intensity correlations of these modes is also preserved, with the size depending on the mode index difference, the information may also be transmitted by means of these correlation pairs.

CRediT authorship contribution statement

K.O. Bastian: Writing – review & editing, Visualization, Validation, Software, Methodology, Investigation, Formal analysis. **S. Pokharel:** Writing – review & editing, Validation, Methodology, Investigation, Formal analysis. **M. Mahdavifar:** Writing – review & editing, Validation, Investigation, Data curation, Conceptualization. **O. Korotkova:** Writing – original draft, Supervision, Project administration, Investigation, Formal analysis, Data curation, Conceptualization.

Declaration of competing interest

The authors declare that they have no known competing financial interests or personal relationships that could have appeared to influence the work reported in this paper.

Acknowledgments

The authors are indebted to S. M. Hashemi Rafsanjani for his help on the experimental aspects of the work.

Data availability

Data will be made available on request.

References

[1] L. Allen, M.W. Beijersbergen, R. Spreeuw, et al., Orbital angular momentum of light and transformation of Laguerre Gaussian laser modes, Phys. Rev. A 45 (1992) 8185—8189.

[2] G. Gibson, J. Courtial, M.J. Padgett, M. Vasnetsov, V. Pas'ko, S.M. Barnett, S. Franke-Arnold, Free-space information transfer using light beams carrying orbital angular momentum, Opt. Express 12 (2004) 5448–5456.

[3] J. Wang, J.Y. Yang, I.M. Fazal, N. Ahmed, Y. Yan, H. Huang, Y. Ren, Y. Yue, S. Dolinar, M. Tur, A.E. Willner, Terabit free-space data transmission employing orbital angular momentum multiplexing, Nat. Photon. 6 (2012) 488–496.

[4] Y. Ren, L. Li, Z. Wang, S. Mahsa Kamali, E. Arbabi, A. Arbabi, Z. Zhao, G. Xie, Y. Cao1, N. Ahmed, Y. Yan, C. Liu, A.J. Willner, S. Ashrafi, M. Tur, A. Faraon, A.E. Willner, Orbital angular momentum-based space division multiplexing for high-capacity underwater optical communications, Sci. Rep. 6 (2016) 33306.

[5] C. Paterson, Atmospheric turbulence and orbital angular momentum of single photons for optical communication, Phys. Rev. Lett. 94 (2005) 153901.

[6] H.F. Elder, P. Sprangle, Mode power spectrum for Laguerre–Gauss beams in Kolmogorov turbulence, Opt. Lett. 47 (2022) 3447–3450.

[7] H.F. Elder, P. Sprangle, Full mode power spectrum for Laguerre-Gauss beams in strong Kolmogorov turbulence, Opt. Express 30 (2022) 45508–45516.

[8] G. Gbur, R.K. Tyson, Vortex beam propagation through atmospheric turbulence and topological charge conservation, J. Opt. Soc. Amer. A 25 (2008) 225–230.

[9] V.P. Lukin, P.A. Konyaev, V.A. Sennikov, Beam spreading of vortex beams propagating in turbulent atmosphere, Appl. Opt. 51 (2012) C84–C87.

[10] V.A. Banakh, A.V. Falits, Turbulent broadening of Laguerre-Gaussian beam in the atmosphere, Opt. Spectrosc. 117 (2014) 942–948.
[11] B. Rodenburg, M.P.J. Lavery, M. Malik, M.N. O'Sullivan, M. Mirhosseini, D.J. Robertson, M. Padgett, R.W. Boyd, Influence of atmospheric turbulence on states of light carrying orbital angular momentum, Opt. Lett. 37 (2012) 3735–3737.
[12] B. Rodenburg, M. Mirhosseini, M. Malik, O.S. Magana-Loaiza, M. Yanakas, L. Maher, N.K. Steinhoff, G.A. Tyler, R.W. Boyd, Simulating thick atmospheric turbulence in the lab with application to orbital angular momentum communication, New J. Phys. 16 (2014) 033020.
[13] N.A. Ferlic, M. van Iersel, C.C. Davis, Weak turbulence effects on different beams carrying orbital angular momentum, J. Opt. Soc. Amer. A 38 (2021) 1423–1437.
[14] J. Zeng, X. Liu, C. Zhao, F. Wang, G. Gbur, Y. Cai, Spiral spectrum of a Laguerre-Gaussian beam propagating in anisotropic non-Kolmogorov turbulent atmosphere along horizontal path, Opt. Express 27 (2019) 25342–25356.
[15] Y. Zhang, C. Ke, Y. Xie, Y. Zhang, Experimental investigation of LG beam propagating in actual atmospheric turbulence, Results Phys. 35 (2022) 105327.
[16] J. Li, X. Chen, S. McDuffie, M. Najjar, S.M.H. Rafsanjani, O. Korotkova, Mitigation of atmospheric turbulence with random beams carrying OAM, Opt. Commun. 446 (2019) 178–185.
[17] J. Rodriguez, D. Montaño, S.M.H. Rafsanjani, O. Korotkova, Mueller matrix of the particle-free atmospheric enhanced backscatter, Opt. Lett. 44 (2019) 5330–5333.
[18] R. Ma, K.H. Luo, S. Pokharel, Z. Wang, O. Korotkova, J.S. He, W.L. Zhang, D.Y. Fan, A.S.L. Gomes, J. Liu, Orbital-angular-momentum dependent speckles for spatial mode sorting and demultiplexing, Optica 11 (2024) 595–605.
[19] D.G. Voelz, Computational Fourier Optics, A MATLAB Tutorial SPIE Press, Washington, 2011.
[20] L.C. Andrews, R.L. Phillips, Laser Beam Propagation in Random Media, second ed., SPIE Press, Washington, 2005.